Journal of Experimental Botany, Vol. 69, No. 15 pp. 3651–3660, 2018
doi:10.1093/jxb/ery141 Advance Access publication 12 April 2018
This paper is available online free of all access charges (see https://academic.oup.com/jxb/pages/openaccess for further details)

RESEARCH PAPER

Inorganic carbon and pH dependency of photosynthetic rates in *Trichodesmium*

Tobias G. Boatman[1,†,*], Niall M. Mangan[2], Tracy Lawson[1] and Richard J. Geider[1]

[1] School of Biological Sciences, University of Essex, Wivenhoe Park, Colchester, Essex, CO4 3SQ, UK
[2] Department of Engineering Sciences and Applied Mathematics, Northwestern University, Evanston, Illinois, 60208, USA

* Correspondence: tboatman@chelsea.co.uk
† Chelsea Technologies Group Ltd, 55 Central Avenue, West Molesey, Surrey KT8 2QZ, UK

Received 13 December 2017; Editorial decision 9 April 2018; Accepted 9 April 2018

Editor: Susanne von Caemmerer, Australian National University, Australia

Abstract

Increasing atmospheric CO_2 concentrations are leading to increases in dissolved CO_2 and HCO_3^- concentrations and decreases in pH and CO_3^{2-} in the world's oceans. There remain many uncertainties as to the magnitude of biological responses of key organisms to these chemical changes. In this study, we established the relationship between photosynthetic carbon fixation rates and pH, CO_2, and HCO_3^- concentrations in the diazotroph, *Trichodesmium erythraeum* IMS101. Inorganic ^{14}C-assimilation was measured in TRIS-buffered artificial seawater medium where the absolute and relative concentrations of CO_2, pH, and HCO_3^- were manipulated. First, we varied the total dissolved inorganic carbon concentration (TIC) (<0 to ~5 mM) at constant pH, so that ratios of CO_2 and HCO_3^- remained relatively constant. Second, we varied pH (~8.54 to 7.52) at constant TIC, so that CO_2 increased whilst HCO_3^- declined. We found that ^{14}C-assimilation could be described by the same function of CO_2 for both approaches, but it showed different dependencies on HCO_3^- when pH was varied at constant TIC than when TIC was varied at constant pH. A numerical model of the carbon-concentrating mechanism (CCM) of *Trichodesmium* showed that carboxylation rates are modulated by HCO_3^- and pH. The decrease in assimilation of inorganic carbon (Ci) at low CO_2, when TIC was varied, was due to HCO_3^- uptake limitation of the carboxylation rate. Conversely, when pH was varied, Ci assimilation declined due to a high-pH mediated increase in HCO_3^- and CO_2 leakage rates, potentially coupled to other processes (uncharacterised within the CCM model) that restrict Ci assimilation rates under high-pH conditions.

Keywords: Carbon acquisition, carbon concentrating mechanism (CCM), CO_2, Cyanobacteria, gross photosynthesis, net photosynthesis, ocean acidification, *Trichodesmium*.

Introduction

Over the past 150 years, atmospheric CO_2 concentrations have increased from pre-industrial levels (i.e. 280 μmol mol^{-1}) to a current value of about 400 μmol mol^{-1}, and are predicted to increase further to 650 μmol mol^{-1} by mid-century, and to 750–1000 μmol mol^{-1} by the end of this century (Raven *et al.*, 2005). Equilibration of CO_2 between the atmosphere and the oceans is leading to increases in dissolved CO_2 and HCO_3^- and to decreases in pH and CO_3^{2-}. This process of ocean acidification is predicted to reduce the pH from average pre-industrial levels of 8.2 to about 7.9 by the end of the century (Zeebe *et al.*, 1999; Zeebe and Wolf-Gladrow, 2001). To date, there are still many uncertainties as to the magnitude of biological responses of key organisms to these chemical changes.

One group of organisms of particular importance are the diazotrophic cyanobacteria (photosynthetic dinitrogen-fixers), notably because of their significant contribution to marine primary productivity by converting N_2 into NH_4^+, thus providing 'new' nitrogen to the oceans. The filamentous cyanobacterium *Trichodesmium* is a colony-forming species that fixes nitrogen in an area corresponding to half the Earth's surface (Davis and McGillicuddy, 2006), and is estimated to account for more than half of the new (combined) nitrogen production in many parts of the oligotrophic tropical and sub-tropical oceans (Capone *et al.*, 2005).

Cyanobacteria, *Trichodesmium* species included, achieve high photosynthetic rates despite (i) the slow diffusion of CO_2 in water (10^4 times slower than in air), (ii) a slow chemical equilibrium between HCO_3^- and CO_2 within the 7–8.5 pH range, and (iii) a low affinity of Rubisco for CO_2 relative to ambient CO_2 concentrations. Cyanobacteria employ an intracellular carbon-concentrating mechanism (CCM) (Badger and Price, 2003; Badger *et al.*, 2006; Kranz *et al.*, 2010), where enhanced primary productivity significantly outweighs the metabolic costs of CCM activity (Price *et al.*, 2008). The CCM benefits cyanobacteria by reducing photorespiration (Schwarz *et al.*, 1995; Kaplan and Reinhold, 1999), aiding in the dissipation of excess light energy, and by maintaining an optimal intracellular pH (Badger *et al.*, 1994; Kaplan and Reinhold, 1999). The general consensus is that up-regulation of CCM activity in response to a low-CO_2 environment involves two components. Firstly, an increase in the transport of inorganic carbon (Ci) from the environment into the cell via a suite of Ci transporters, which could involve using ATP (BCT1 HCO_3^- transporter), NADPH, or reduced ferredoxin (CO_2 conversion from passive diffusion) or coupling to an electrochemical Na^+ gradient (SbtA or BicA HCO_3^- transport) to provide the energy for Ci uptake (Badger *et al.*, 2002; Badger and Price, 2003). Secondly, an increased ability to reduce CO_2 leakage from around the site of carboxylation, achieved via arrangement of the molecular components of the carboxysome structure and a CO_2-uptake system located on the thylakoid layer, preventing the efflux of leaked CO_2 to the outer cytosolic layer (Price *et al.*, 2008).

Both ^{14}C isotope disequilibrium experiments and simultaneous measurements of CO_2 and O_2 exchanges during sequential light–dark transitions indicate that HCO_3^- contributes >90% of the Ci assimilation by *T. erythraeum* IMS101 (Kranz *et al.*, 2009; Eichner *et al.*, 2015). This preference for HCO_3^- is consistent with the evidence that *Trichodesmium* lacks a plasma membrane-bound extracellular carbonic anhydrase (eCA) (Badger *et al.*, 2006; Price *et al.*, 2008). Furthermore, the *T. erythraeum* genome indicates the presence of both a plasma membrane HCO_3^- transporter (BicA) and an intracellular system for conversion of CO_2 to HCO_3^- (NDH-I_4) (Price *et al.*, 2008). These two modes of the CCM result in the accumulation of HCO_3^- in the cytosol, which diffuses to the carboxysome. Inorganic carbon uptake by *Trichodesmium* involves the uptake of HCO_3^- by the BicA transporter. This transporter has a half-saturation constant, K_m, of 40–100 μM HCO_3^-, which is well below the typical concentration of HCO_3^- in seawater (~2000 μM) (Badger *et al.*, 2006). Following transport into the cell, C-fixation in *Trichodesmium*, like other cyanobacteria species, occurs within carboxysomes where HCO_3^- is converted to CO_2 via a carbonic anhydrase, followed by fixation of CO_2 by Rubisco. Carboxysomes provide micro-environments where CO_2 is elevated to compensate for the low affinity of cyanobacterial Rubiscos for CO_2 (K_mCO_2>150 mM) (Badger and Andrews, 1987). In *Trichodesmium*, CO_2 that leaks from carboxysomes can be converted to HCO_3^- by the plasma membrane-bound NDH-I_4 protein, thus reducing the efflux of CO_2 from the cell, but at a cost of consuming reducing equivalents (NADPH or reduced Fd) (Price *et al.*, 2008). Despite having a mechanism for intracellular recycling of CO_2, efflux is reported to account for the loss of up to 50% of HCO_3^- uptake in *Trichodesmium* (Kranz *et al.*, 2010; Eichner *et al.*, 2015).

As reviewed in Boatman *et al.* (2017), the majority of previous studies have shown an increase (albeit not all statistically significant) in *T. erythraeum* IMS101 growth under predicted future CO_2 concentrations (~750–1000 μmol mol^{-1}), although the magnitudes of these responses differ between studies (see Supplementary Table S1 at *JXB* online). The increased growth and productivity of *T. erythraeum* IMS101 with increased CO_2 is probably attributable to a decrease in the energy required for operation of the CCM, allowing more energy (ATP) and reductant (NADPH) to be reallocated to N_2 fixation, CO_2 fixation, and biosynthesis (Kranz *et al.*, 2011).

Given the significant contribution of *Trichodesmium* to carbon and nitrogen biogeochemical cycles, and the predicted changes to Ci speciation over the coming decades due to ocean acidification, we performed a systematic study to assess how the kinetics of Ci assimilation of *T. erythraeum* IMS101 were affected by acclimation to varying CO_2 concentrations. We ensured that the Ci chemistry and all other growth conditions were well defined, with cultures fully acclimated over long time periods to achieve balanced growth. We assessed how the rate of Ci assimilation was related to CO_2 or HCO_3^- concentrations in experiments where Ci speciation was modulated by varying pH and total dissolved inorganic carbon concentration (TIC). These assays of photosynthetic performance showed that *Trichodesmium* productivity was influenced by high pH when TIC was held at a saturating concentration, indirectly making the rate of Ci assimilation a saturating function of CO_2 concentration, and that maximum rates of CO_2 fixation declined and affinity for CO_2 increased when *Trichodesmium* was acclimated to a low-CO_2 concentration. We discuss how these responses can be attributed to decreases in the cost of operating a CCM under future CO_2 conditions.

Materials and methods

Trichodesmium erythraeum IMS101 was semi-continuously cultured to achieve fully acclimated balanced growth at three target CO_2 concentrations (180, 380, and 720 μmol mol^{-1}) under saturating light intensity (400 μmol photons m^{-2} s^{-1}), a 12/12 h light/dark (L/D) cycle, and an optimum growth temperature (26 ± 0.7 °C) for ~5 months (~80 generations).

Experimental set-up

Cultures of *T. erythraeum* IMS101 were grown using YBCII medium (Chen *et al.*, 1996) at 1.5-l volumes in 2-l Pyrex bottles that had been acid-washed and autoclaved prior to culturing. Daily growth rates were quantified from changes in baseline fluorescence (F_o) measured between 09.00 to 10.30 h on dark-adapted cultures (20 min) using a FRRfII FastAct Fluorometer System (Chelsea Technologies Group Ltd, UK). Cultures were kept at the upper section of the exponential growth phase through periodic dilution with new growth media at 3–5 d intervals. They were deemed fully acclimated and in balanced growth when both the slope of the linear regression of $\ln(F_o)$ and the ratio of live-cell to acetone-extracted (method detailed below) baseline fluorescence were constant following every dilution with fresh YBCII medium. Illumination was provided side-on by fluorescent tubes (Sylvania Luxline Plus FHQ49/T5/840). Cultures were constantly mixed using magnetic PTFE stirrer bars and aerated with a filtered (0.2-μm pore) air mixture at a rate of ~200 ml s^{-1}. The CO_2 concentration was regulated (±2 μmol mol^{-1}) by mass-flow controllers (Bronkhorst, Newmarket, UK) and CO_2-free air was supplied by an oil-free compressor (Bambi Air, UK) via a soda-lime gas-tight column that was mixed with a 10% CO_2-in-air mixture from a gas cylinder (BOC Industrial Gases, UK). The CO_2 concentration in the gas phase was continuously monitored and recorded by an infra-red gas analyser (Li-Cor Li-820, Nebraska USA), calibrated weekly against a standard gas (BOC Industrial Gases).

The Ci chemistry was measured prior to the dilution of each culture with fresh media; pH and TIC were measured directly, while HCO_3^-, CO_3^{2-}, and CO_2 concentrations were calculated using CO2SYS with the same constants as described in Boatman *et al.* (2017) (see Supplementary Information SI).

Elemental stoichiometry

Samples for elemental composition and CO_2-response curves were collected at the same time of day between 4 and 6 h into the light period of the L/D cycle. Samples for determination of particulate organic carbon (POC), particulate nitrogen (PN), and particulate phosphorus (PP) were collected together with each CO_2-response curve, where each sample was a biological replicate culture. Three 100-ml aliquots from each culture were vacuum-filtered onto pre-combusted 25-mm (0.45-μm pore) glass-fibre filters for measurements of POC, PN, and PP. The POC and PN filters were placed in 1.8-ml cryovials (lids off) and dried at 60 °C. The PP filters were rinsed with 2 ml of sodium sulphate (0.1 M), placed in a 20-ml glass scintillation vial, 2 ml of magnesium sulphate (0.017 M) added, and then dried at 60 °C. POC was quantified using a TC analyser (Shimadzu TOC-V Analyser & SSM-5000A Solid Sample Combustion Unit), PN by the method of Bronk and Ward (2000), and PP by the method of Solorzano and Sharp (1980).

Inorganic carbon fixation-response curves

The dependencies of CO_2 fixation on CO_2 and HCO_3^- were determined from experiments that involved varied TIC with fixed pH and varied pH with fixed TIC (see Supplementary Information SII, SIII) in TRIS-buffered YBCII medium using the ^{14}C uptake technique (Steemann Nielsen and Jensen, 1957).

Prior to each experiment, 1 l of bicarbonate-free YBCII medium was aerated overnight with CO_2-free air (soda-lime column). A 200-ml sample from each culture was gravity-filtered onto a 47-mm cyclopore filter (1-μm pore; Whatman 60750) and gently re-suspended into 50 ml of the CO_2-free YBCII medium. Exactly 5 ml of concentrated culture was pipetted into each tube of the TIC or pH gradients (35 ml total volume per tube) and gently inverted to evenly distribute the trichomes. The remaining culture was used for measurement of initial activity, T_0. Three replicate cultures were used per treatment. During sample preparation, test-tubes were maintained at growth temperature (26 °C) and a low light intensity (<10 μmol photons m^{-2} s^{-1}).

To characterise the Ci chemistry, exactly 20 ml of culture from each treatment was filtered through a Swinnex filter (25 mm, 0.45-μm pore, glass-fibre filter): 15 ml into a plastic centrifuge tube (no headspace) for TIC analysis (Shimadzu TOC-V Analyser & ASI-V Autosampler), and 5 ml into a plastic cryogenic vial (Sigma-Aldrich V5257-250EA; no headspace) for pH analysis.

To measure chlorophyll *a* concentrations, a 1-ml sample from each treatment was pipetted into 9 ml of 100% acetone and left in a freezer (–20 °C) overnight (Welschmeyer, 1994). The sample was vortex-mixed and left in the dark (~30 min) to allow cell debris to precipitate and the solution to equilibrate to room temperature. A 2-ml aliquot was used to measure F_o using a FRRfII FastAct Fluorometer System (Chelsea Technologies Group Ltd, UK) with the same parameters as used for live cultures. Chlorophyll *a* concentrations were calculated from a calibration curve derived from a dilution series measured using a chlorophyll *a* standard (Sigma-Aldrich C5753).

To assess whether cells had been affected by concentration via filtration and re-suspension and exposure to the range of TIC and pH gradients over the course of the ^{14}C incubations, 2-ml aliquots of culture from each treatment were dark-acclimated (~20 min) and the photosynthetic efficiency of PSII (F_v/F_m) was determined using a FRRfII FastAct Fluorometer System (Chelsea Technologies Group Ltd, UK) (see Supplementary Fig. S1).

Finally, 10 ml of culture from each treatment was pipetted into 12-ml glass (PTFE-capped) test-tubes and used for ^{14}C incubations. A ^{14}C spike solution was prepared by pipetting 45 μl of a ^{14}C-labelled sodium bicarbonate solution ($NaH^{14}CO_3$) with a specific activity of 52 mCi $mmol^{-1}$ (Perkin Elmer, USA) into 8 ml of bicarbonate-free YBCII media. Exactly 250 μl of the spike was added to each tube culture. The T_0 tubes were immediately filtered through Swinnex filters containing 25-mm diameter (0.45-μm pore) glass-fibre filters, placed in scintillation vials, and acidified (500 μl of 3 M HCl). To determine the total activity (TC), 20 μl of the spike was added into three scintillation vials already containing 4.5 ml of scintillation cocktail (Gold LLT) and 200 μl of phenylethylamine. The TC vial caps were screwed tight immediately. The spiked test-tubes were placed within a custom-made water-jacketed incubator and maintained at 26 °C under saturating light intensity (400 ± 6 μmol photons m^{-2} s^{-1}) (The Optoelectronic Manufacturing Corporation Ltd. 1ft T5 Daylight, UK). The incubations lasted between 60 and 90 min and took place between 4 to 6 h into the light period of the L/D cycle. The ^{14}C incubations were repeated in the dark, using black-coated (Plasti-Kote paint) test-tubes. Dark ^{14}C uptake rates were 8.25% (±0.46) and 7.05% (±0.25) of the maximum light-saturated ^{14}C uptake rates for the TIC and pH response curves, respectively. Dark ^{14}C uptake rates exhibited no response to varying TIC or pH and were used to correct the light-dependent rates of photosynthesis (Li and Dickie, 1991).

To terminate ^{14}C uptake, samples were filtered through 25-mm (0.45-μm pore) glass-fibre filters (Fisherbrand FB59451, UK) using a bespoke 30-funnel filtration manifold. Test-tubes and filters were rinsed twice with 5 ml of YBCII media, before the filters were placed into scintillation vials. The vials were acidified (500 μl of 3 M HCl) overnight along with the T_0 samples. Exactly 4.5 ml of scintillation cocktail (Gold LLT) was added to the acidified vials and the caps tightened. Ensuring that the scintillation cocktail and filtered samples were well mixed, the vials were placed within a scintillation counter and the disintegrations per minute (DPM) of each vial were measured (20 min per vial). The CO_2 fixation rates were calculated using the following equation:

$$\text{C}-\text{fixation} = \left(\frac{\text{DPM}_\text{S} - \text{DPM}_{\text{T0}}}{\text{DPM}_{\text{TC}}}\right) \times \left(\frac{\text{Vol}_{\text{TC}}}{\text{Vol}_\text{s}}\right) \times \left(\frac{\text{TIC}}{t}\right) \times 1.05 \quad (1)$$

where DPM_S, DPM_{T0}, and DPM_{TC} are the measurements for the sample, initial activity, and total activity vials, respectively; TIC (mmol l^{-1}) is the mean concentration of total dissolved inorganic carbon within the sample over the course of the incubation (inclusive of the $NaH^{14}CO_3$ spike); Vol_{TC} and Vol_S are the volumes of the sample and TC vials, respectively; t is the experimental incubation time (h); and 1.05 is the radioisotope discrimination factor (^{12}C:^{14}C). Note that mean T_0 and TC values were used when calculating the C-fixation rates (n=3).

Inorganic carbon fixation rates were normalised to a POC basis and the CO_2 response curves were fitted to a Michaelis–Menten function:

$$V_\text{C} = \frac{\left(V_{\text{C,max}} \cdot [CO_2]\right)}{\left(K_\text{m} + [CO_2]\right)} \quad (2)$$

where V_C is the organic C-specific rate of CO_2 fixation, $V_{C,max}$ is the maximum rate of CO_2 fixation, and K_m is the half-saturation constant. Curve-fitting was performed on individual replicates to calculate mean (±SE) curve-fit parameters (Sigmaplot 11.0), as well on the combined data where all replicates of the varied TIC (fixed pH) and varied pH (fixed TIC) data were combined per CO_2 treatment.

Spectrophotometric chlorophyll a analysis

Samples for spectrophotometric determination of chlorophyll *a* were collected together with each CO_2-response curve and were used to normalise productivity rates as well as to calculate the ratio of Chl *a*:C (i.e. total C). A 100-ml sample from each culture was vacuum-filtered onto a 25-mm (0.45-µm pore) glass-fibre filter (Fisherbrand FB59451, UK) and extracted in 5 ml of 100% methanol. The filters were homogenised and extracted overnight at –20 °C before being centrifuged at 12 000 *g* for 10 min and a 3-ml aliquot of the supernatant was transferred to a quartz cuvette. The absorption spectrum (400–800 nm) was measured using a spectrophotometer (Hitachi U-3000, Japan) and the Chl *a* concentration (µg l^{-1}) was calculated using the following equation (Ritchie, 2008);

$$\text{Chl } a = \left(\frac{12.9447 \times (\text{Abs}_{665} - \text{Abs}_{750}) \times \text{Vol}_E}{\text{Vol}_F} \right) \times 1000 \quad (3)$$

where Abs_{665} and Abs_{750} are the baseline-corrected optical densities of the methanol extracted sample at 665 and 750 nm, respectively; Vol_E is the volume of the solvent used for extraction (i.e. 5 ml); Vol_F is the volume of culture that was filtered (i.e. 100 ml); and 12.9447 is a cyanobacteria-specific Chl *a* coefficient for 100% methanol extraction.

Modelling the CCM

The CO_2 and HCO_3^- fluxes and concentrations in an idealised *Trichodesmium* cell were calculated using the numerical model from Mangan *et al.* (2016) and Mangan and Brenner (2014). The aim was to provide a qualitatively informative view of the CCM system, without attempting to match carboxylation rates or fluxes to the experimental system or to rescale the results from the idealised cell to what would be expected from the experimental data. With the exception of a few key parameter values (Table 1), the model used was equivalent to that reported in Mangan *et al.* (2016). The main changes between the idealised *Trichodesmium* cell and previous models were an increase in cell and carboxysome size to be consistent with reported values for *T. erythraeum*, changes to the Rubisco kinetic constants, use of pH and external CO_2 and HCO_3^- concentrations similar to those in the ^{14}C incubations, updating the pKa_{eff} for HCO_3^- to CO_2 to match that used in the CO2SYS calculation, and re-calculating the HCO_3^- uptake rate to support internal inorganic carbon concentrations of ~30 mM. We scaled the Rubisco concentration by the carboxysome volume, so that the activity per volume remained the same. Similarly, we scaled the amount of carbonic anhydrase by the carboxysome surface area, so that the activity per area remained the same. The carbonic anhydrase activity was sufficient to equilibrate CO_2 and HCO_3^- to $K'_{eq} = [HCO_{3^-}]/[CO_2] = 10^{-pKa_{eff}+pH}$. We set the carbonic anhydrase K_{ca} value to preserve the correct equilibrium value for the internal pH.

Table 1. *Key parameter values used in the numerical simulation of the CCM in* Trichodesmium

Variable	Units	Model value
Cell radius, R_b	µm	3
Carboxysome radius, R_c	µm	0.15
Rubisco reaction rate, k_{Rub}	s^{-1} per active site	1.92
Rubisco K_{CO2}	µM	145
Rubisco K_{O2}	µM	600
Rubisco specificity, S	–	45
Number of Rubisco active sites	–	54000
Number of carbonic anhydrase active sites	–	900
Carbonic anhydrase half-maximum constant for CO_2, K_{ca}	µM	104.7
Internal pH	–	8.3
pKa_{eff} for HCO_3^-:CO_2	–	5.84
Carboxysome permeability	cm s^{-1}	3×10^{-5}
HCO_3^- uptake velocity, j_c	cm s^{-1}	2.4×10^{-7}
CO_2 to HCO_3^- conversion at membrane	cm s^{-1}	0.6×10^{-7}

The cell radius was measured from a bioimage collected using fluorescence microscopy (Supplementary Fig. S12). Kinetic constants of Rubisco carboxylation (K_{CO2}), oxygenation (K_{O2}), and the specificity factor (S) for a form 1B cyanobacteria were taken from Badger *et al.* (1998).

Results

Inorganic carbon chemistry, growth rate, and cell composition

Overall, the CO_2 drawdown in the cultures ranged between 57–78 µmol mol^{-1} for all CO_2 treatments (Table 2) and exhibited a negligible CO_2 drift over a diurnal cycle (see Supplementary Fig. S2). Dissolved inorganic NH_4^+ concentrations in the growth medium were ~1 µM, while NO_3^- concentrations were ~0.3 µM, which was below the 1 µM detection limit.

Balanced growth rates increased from ~0.2 d^{-1} at low CO_2 to ~0.34 d^{-1} at mid-CO_2 and ~0.36 d^{-1} at high CO_2 (Table 3). The dark-adapted photochemical efficiencies of PSII (F_v/F_m) were proportionate to the CO_2 treatment, increasing from 0.27 at low CO_2 to ~0.31 at mid-CO_2 and ~0.34 at high CO_2 (Table 3). The particulate C:N ratio was independent of CO_2, while the C:P and N:P ratios increased with increasing CO_2 (Table 3). Both Chl *a*:C and Chl *a*:N ratios were about 30–40% higher at mid-CO_2 than at low or high CO_2.

CO_2-response curves

Based on the shape of the response curves, the inorganic carbon (^{14}C) fixation rate was fitted to a saturating function of the dissolved CO_2 concentration in both the pH gradient and TIC gradient experiments (Fig. 1). Although a saturating function of HCO_3^- concentration was observed when TIC was varied at constant pH (Fig. 1A–C), Ci assimilation could not be described by the same kinetic constants when pH was varied at constant TIC (Fig. 1D–F).

The K_m for photosynthetic C-fixation increased from 0.8 µM in cultures acclimated to low CO_2 to 2.2 µM and 3.2 µM in cultures acclimated to mid- and high CO_2, respectively, and were approximately 4- to 5-fold lower than the ambient CO_2 concentrations in the cultures. The maximum organic carbon-specific rate of C-fixation ($V_{C,max}$) was also higher in cells grown at mid-CO_2 than at low CO_2, although the rates at mid- and high CO_2 did not differ significantly (Table 4). The affinity for CO_2 ($V_{C,max}/K_m$) declined by about 40% between the low- and high-CO_2 treatments (Table 4).

Table 2. *The growth conditions (±SE) achieved for* T. erythraeum *IMS101 when cultured at three target gas-phase CO_2 concentrations (Low=180 µmol mol^{-1}, Mid=380 µmol mol^{-1}, and High=720 µmol mol^{-1}), saturating light intensity (400 µmol photons m^{-2} s^{-1}), and optimal temperature (26 °C)*

Variable	Units	Low CO_2	Mid CO_2	High CO_2
pH	–	8.458	8.174	7.906
H^+	nM	3.5 (0.20)	6.7 (0.13)	12.4 (0.28)
A_T	µM	2431 (70)	2447 (54)	2442 (56)
TIC	µM	1800 (69)	2039 (46)	2201 (50)
HCO_3^-	µM	1362 (67)	1743 (39)	2005 (44)
CO_3^{2-}	µM	435 (16)	289 (9)	179 (6)
CO_2	µM	3.3 (0.3)	8.1 (0.2)	17.3 (0.5)
NH_4^+	µM	1.03 (0.14)	1.00 (0.08)	1.08 (0.06)
NO_3^-	µM	0.34 (0.05)	0.32 (0.03)	0.30 (0.02)
n		89	67	39

Individual pH values were converted to a H^+ concentration, allowing a mean pH value (Total scale) to be calculated. Dissolved inorganic NH_4^+ was determined using the phenol-hypochlorite method as described by Solorzano (1969), while dissolved inorganic NO_3^- was determined using the spectrophotometric method as described by Collos *et al.* (1999).

Table 3. *The mean (±SE) balanced growth rate, dark-adapted photochemical efficiency of PSII (F_v/F_m), elemental stoichiometry, and chlorophyll* a *to C and N ratios for* T. erythraeum *IMS101 when acclimated to three target CO_2 concentrations (Low=180 µmol mol^{-1}, Mid=380 µmol mol^{-1}, and High=720 µmol mol^{-1}), saturating light intensity (400 µmol photons m^{-2} s^{-1}), and optimal temperature (26 °C)*

Variable	Units	Low CO_2	Mid CO_2	High CO_2
Growth rate	d^{-1}	0.198 (0.027)^A	0.336 (0.026)^B	0.361 (0.020)^B
F_v/F_m	dimensionless	0.274 (0.025)^A	0.305 (0.020)^B	0.342 (0.037)^C
Elemental stoichiometry				
C:N	mol:mol	7.9 (0.8)	7.8 (0.3)	7.3 (0.8)
C:P	mol:mol	91.9 (6.3)^A	143.6 (6.3)^B	155.5 (13.5)^B
N:P	mol:mol	11.9 (0.6)^A	18.4 (0.7)^B	21.8 (1.7)^B
Chl *a*:C	g:mol	0.052 (0.003)^A	0.089 (0.003)^C	0.066 (0.003)^B
Chl *a*:N	g:mol	0.401 (0.037)^A	0.693 (0.035)^B	0.474 (0.043)^A

Replicates comprised *n*=9 at low CO_2, *n*=6 at mid- and high CO_2. Letters indicate significant differences between CO_2 treatments (one-way ANOVA, Tukey *post hoc* test; $P<0.05$); where B is significantly greater than A, and C is significantly greater than B and A.

Modelled response curves

Without parameter-fitting, the CCM model of *Trichodesmium* produced behaviors consistent with the experimental data when either external TIC (i.e HCO_3^-) was varied at a fixed pH or when pH was varied at a fixed TIC (Fig. 2A, B). Assuming HCO_3^- is the dominant form of inorganic carbon taken up by the cell (Kranz *et al.*, 2009; Eichner *et al.*, 2015), *Trichodesmium* exhibited a significant response to changes in external pH and CO_2 concentrations. The decrease in carboxylation rate with decreasing external CO_2 was due to a decrease in HCO_3^- uptake (when TIC was varied) or an increase in HCO_3^- and CO_2 leakage out of the cell (when pH was varied) (Supplementary Fig. S3). Modelled carboxylation rates from both numerical simulations exhibited a smooth function of HCO_3^- uptake, HCO_3^- leakage, and CO_2 leakage (Fig. 2C).

The $V_{C,max}$ of the pH gradient and TIC gradient experiments were not significantly different (Supplementary Table S3). However, the maximum carboxylation rates from the simulations were significantly different (Fig. 2); principally because the external HCO_3^- concentration used in the pH-dependent simulation (chosen to be the same as the experiment) was not sufficient to saturate Rubisco. It is possible that the K_m value assumed for Rubisco was set too high, or the internal pH, geometry, or HCO_3^- uptake values were substantially different. Note that we were simulating values beyond the range of those in the experiments, so such a discrepancy is magnified.

Discussion

The key findings of our study were as follows. The acclimated growth rate increased from low- to mid-CO_2 treatments but did not increase significantly between mid- and high-CO_2, suggesting that the positive effect of elevated CO_2 on *Trichodesmium* carbon assimilation over the coming decades may only be slight. The maximum rate ($V_{C,max}$) and the half-saturation constant (K_m) for C-fixation increased with increasing CO_2 treatment, but the affinity for CO_2 ($V_{C,max}/K_m$) declined, which is probably attributable to the activity of the CCM in *Trichodesmium*. The measured inorganic C-fixation rate in *Trichodesmium* could be described as a saturating function of CO_2, both when CO_2 was manipulated by varying pH at constant TIC and when CO_2 was manipulated by varying TIC at constant pH. A mechanistic model of the CCM in *Trichodesmium* indicated that the former was due to HCO_3^- uptake limitation of carboxylation rate, whereas the latter was due to a high-pH-mediated increases in HCO_3^- and CO_2 leakage, potentially coupled to other unknown processes operating

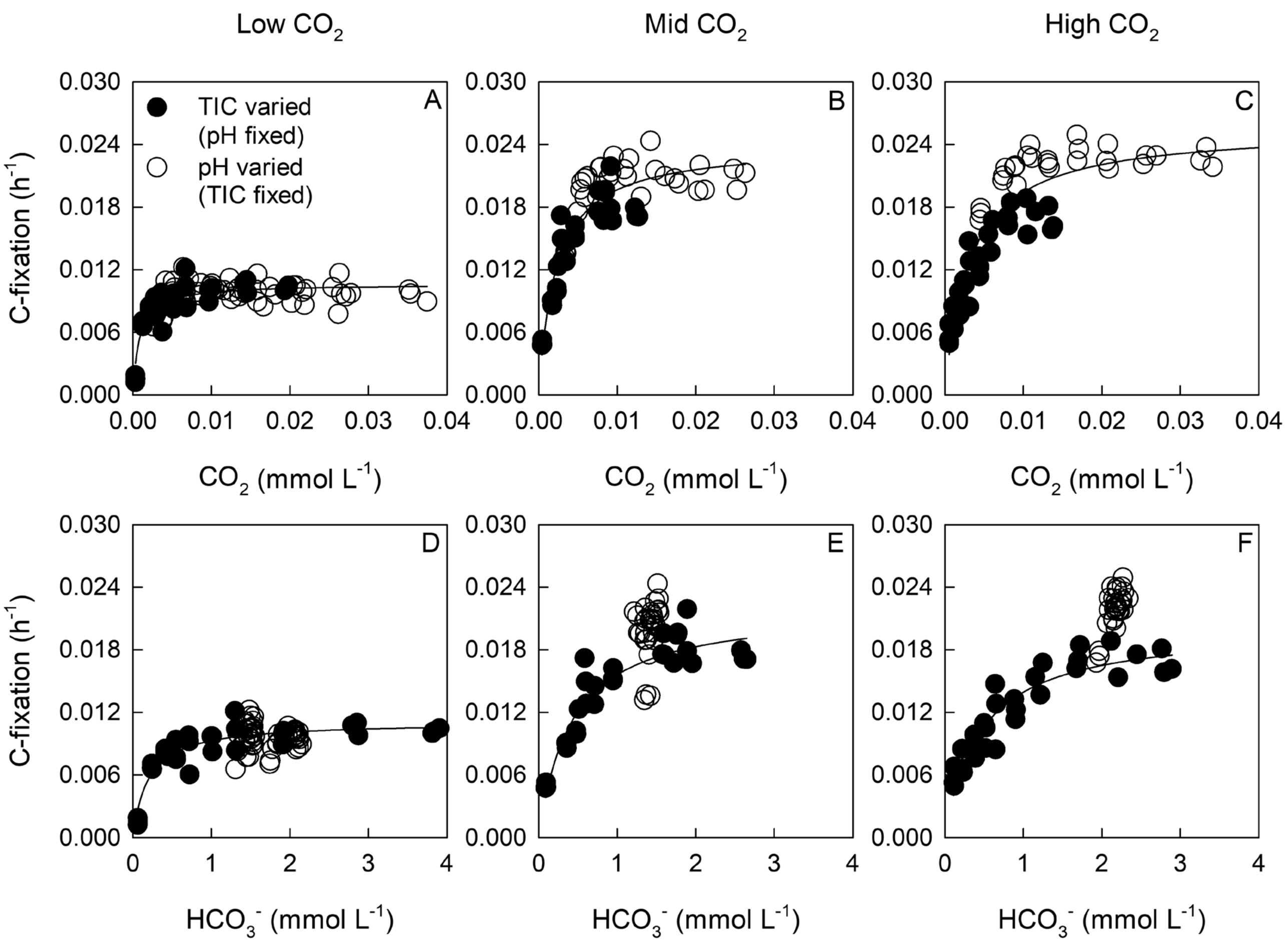

Fig. 1. (A–C) CO_2- and (D–F) HCO_3^--response curves for inorganic C-fixation by *T. erythraeum* IMS101. C-fixation rates are normalised to a carbon h^{-1} basis. Filled circles indicate data obtained by varying TIC and HCO_3^- at a fixed pH of ~8.15. Open circles indicate data obtained by varying pH (~7.52–8.54) at a fixed TIC. Differences in the range of HCO_3^- and CO_2 gradients between CO_2 treatments were due to variability in pipetting and not from instability in the Ci chemistry. For the CO_2 response, curve-fitting was performed using all replicates from both the TIC and pH gradients. For the HCO_3^- response, curve-fitting was performed using data from the TIC gradient only. The CO_2- and HCO_3^-- response curves for individual experiments are shown in Supplementary Figs S6–S11.

Table 4. *The physiological parameters (±SE) of the C-specific C-fixation versus CO_2 concentration response curves for* T. erythraeum *IMS101, fitted using the Michaelis–Menten model to obtain estimates using the combined data from all replicates from both experiments employing varied TIC at fixed pH and varied pH at fixed TIC for each CO_2 treatment*

Parameter	Units	Low CO_2	Mid CO_2	High CO_2
$V_{C,max}$	h^{-1}	0.011 (0.0002)	0.024 (0.0007)	0.026 (0.0008)
K_m	µM CO_2	0.8 (0.1)	2.2 (0.3)	3.2 (0.4)
Affinity	mM $(CO_2)^{-1}$ h^{-1}	13.3 (1.7)	10.9 (1.5)	8.0 (1.0)

$V_{C,max}$, the C-specific maximum C-fixation rate; K_m, the half saturation constant; Affinity, the C-specific initial slope of the $V_{C,max}$ versus CO_2-response curve.

outside of the paramaterised model that were restricting Ci assimilation rates at high pH. Such processes may involve the direct effect of pH on membrane conformation, membrane transport processes, or metabolic functions.

Effect of acclimation to variations in inorganic chemistry on growth rates and elemental stoichiometry

The increased growth rates that we observed from low- (180 µmol mol^{-1}) to mid- (380 µmol mol^{-1}) and high-CO_2 treatments (720 µmol mol^{-1}) were similar to previous findings (Barcelos e Ramos *et al.*, 2007; Boatman *et al.*, 2017, 2018*b*). The growth rate at high CO_2 was 8% greater than at mid-CO_2, but this difference was not statistically significant. The magnitude of this increase at high CO_2 was comparable to several recent studies, which report growth rate increases of 7–26% with increases of CO_2 beyond 400 µmol mol^{-1} (Barcelos e Ramos *et al.*, 2007; Hutchins *et al.*, 2007; Levitan *et al.*, 2007; Kranz *et al.*, 2010; Garcia *et al.*, 2011; Boatman *et al.*, 2017).

The observed increases in C:P and N:P were consistent with previous findings (Barcelos e Ramos *et al.*, 2007; Kranz *et al.*, 2010; Levitan *et al.*, 2010), with changes that can be ascribed

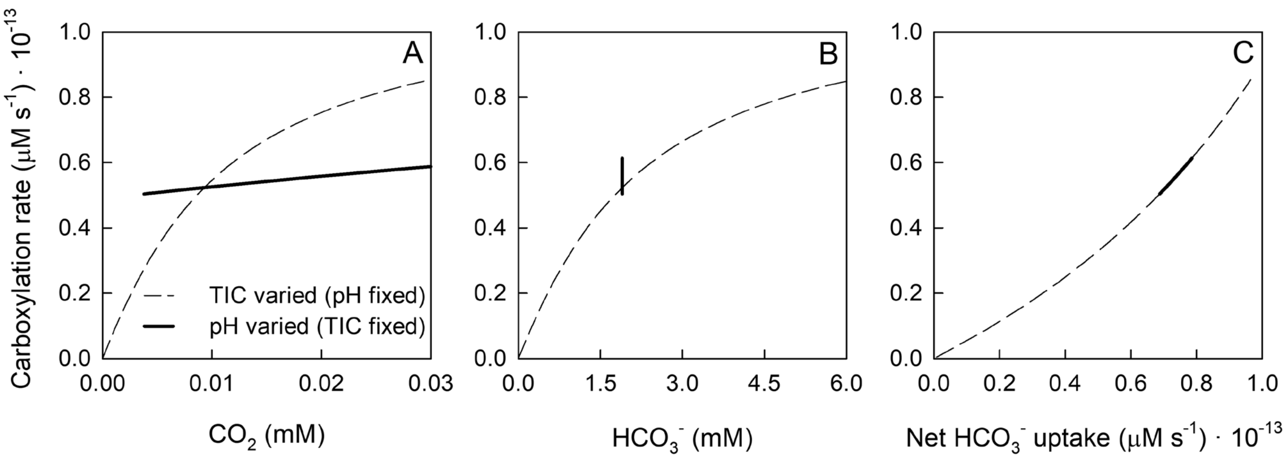

Fig. 2. Calculated carboxylation rates obtained from model simulations for *T. erythraeum* IMS101 as a function of external CO_2 (A) and HCO_3^- (B) concentrations, with TIC (i.e. HCO_3^-) varied at a fixed pH=8.15 (dashed lines) and pH varied at a fixed HCO_3^-=1.9 mM (solid lines). Carboxylation rates are also plotted against the net HCO_3^- uptake rate (C), where HCO_3^- and CO_2 leakage rates were subtracted from the rate of gross HCO_3^- transport.

to increases in cellular N and C incorporation, with P content relatively unaffected by CO_2 (Hutchins *et al.*, 2007; Kranz *et al.*, 2010). In contrast, the C:N ratio and thus the balance between CO_2 fixation and N_2 fixation was not significantly affected by the CO_2 treatment. Similarly, Levitan *et al.* (2007) found that C:N varied only slightly (from 6.5 to 7.0) across growth CO_2 concentrations ranging from 250 to 900 μmol mol^{-1}.

We report C-specific rates here as these are most directly related to changes in specific growth rate because both rates can be expressed in equivalent units of inverse time (e.g. h^{-1} or d^{-1}). However, we note that due to differences in the Chl *a*:C ratio, chlorophyll *a*-specific rates showed a different pattern, increasing progressively from low through mid- to high CO_2 (see Supplementary Table S2, Supplementary Fig. S4). A reduction in Chl *a*:C decreases the energy demands associated with synthesis of the photosynthetic apparatus and is dictated by the total demands for reductant (NADPH) and high-energy phosphate bonds (ATP) (Geider *et al.*, 2009), the minimum turnover times for PSII (τ_{PII}') and PSI (τ_{PI}'), and the minimum pigment content required for effective light absorption and energy transfer (a_{min}') (Behrenfeld *et al.*, 2008). We suggest that the reduced Chl *a*:C at low CO_2 relative to mid-CO_2 was probably due to the cost of up-regulating the CCM, whereas the reduced Chl *a*:C at high CO_2 may have been due to an increase in carbohydrate storage granules relative to the mid-CO_2 treatment (Table 3).

CO_2-response curves

The growth rates reported here were comparable to the 2-μM EDTA, iron-replete (unchelated) treatments in Boatman *et al.* (2017), as well as 20-μM EDTA, iron-replete (chelated) cultures (Boatman *et al.*, 2018*b*), which suggests that our cultures were not exposed to toxic concentrations of certain trace metals (e.g. copper) caused from low trace metal buffering capacity, as reported by Hong *et al.* (2017). Furthermore, dissolved inorganic NH_4^+ concentrations were consistently around 1.0 μM (Table 2). We are therefore confident that the observed positive effect of ocean acidification on growth and primary productivity is driven by the increased CO_2 concentration, rather than being a consequence of a pH-induced shift of the NH_3/NH_4^+ equilibrium. We determined CO_2-response curves at one time of day (4–6 h into the photoperiod of a 12/12 h L/D cycle) and as such cannot extrapolate to a diel response given the reports of temporal separation of photosynthesis and N_2 fixation in *Trichodesmium* (Berman-Frank *et al.*, 2001).

The mechanistic model of Mangan *et al.* (2016) indicates that the CO_2 response we observed when the TIC was varied (pH fixed) was caused by HCO_3^- limitation, where HCO_3^- uptake limits the rate of carboxylation. Conversely, the CO_2 response we observed when pH was varied (TIC fixed) was a function of the pH dependency of HCO_3^- and CO_2 leakage, which in turn could lead to CO_2 limitation of C-fixation and/or diversion of reducing equivalents from powering CO_2 fixation via the Calvin cycle to powering the conversion of CO_2 to HCO_3^- by the NDH-I_4 complex. The model of the CCM in *Trichodesmium* showed the relative importance of leakage, which is notably sensitive to certain parameters in the system such as internal pH, Rubisco activity, cell size, and carboxysome size.

Previous studies have shown a notable response in CCM activity to changes in CO_2; for example, a two-fold lower dissolved inorganic carbon half-saturation concentration in cells acclimated to 150 μmol mol^{-1} (pH 8.56) compared with 370 μmol mol^{-1} (pH 8.26) (Kranz *et al.*, 2009). Our experimental observations indicated that Ci assimilation (V_C) was well described by a CO_2-response curve, but not by a single HCO_3^--response curve (Fig. 1). We now offer an explanation as to the response of V_C to HCO_3^- concentration in the experiments where we varied pH from 7.65 to 8.5 at constant TIC.

Based on the numerical simulations, carboxylation rates across an external pH gradient ranging from 7.5 to 8.5 exhibited a clear linear response, which could not be ascribed to a Michaelis–Menten function (see Supplementary Fig. S3). Conversely, our experimental data showed a clear and significant decrease in Ci assimilation rates at low external CO_2/high pH (Fig. 1). In addition, the Ci assimilation rates for the pH-gradient and TIC-gradient experiments, for all replicates of all three CO_2 treatments, exhibited similar inflection points to external CO_2 (Supplementary Fig. S5). In order for the simulated system to exhibit a rate-saturating response to external CO_2, CO_2 would have to be the dominant source of inorganic carbon. This would contradict all previous research showing that HCO_3^- accounts for >90% of inorganic carbon uptake (Kranz *et al.*, 2009, 2010) and the currently accepted mechanism of Ci assimilation in *T. erythraeum* IMS101 (Badger and Price, 2003).

Given how well the numerical simulations modelled carboxylation rates as a smooth function of HCO_3^- uptake, HCO_3^- leakage, and CO_2 leakage (Fig. 2C), we propose that the linear pH-dependency of carboxylation rate predicted by the model is mechanistically correct, but that processes not captured by the model are contributing to the decrease in Ci assimilation rate at high pH. Such factors could include a direct effect of high pH on cell membrane properties and alteration in membrane conformation (Myklestad and Swift, 1998), or the influence of pH on membrane transport processes and metabolic functions involved in cellular pH regulation (Raven, 1981).

Interestingly, for the mid- and high-CO_2 treatments, a Michaelis–Menten function provided a better fit for the pH-varied (TIC fixed) data than a linear regression. However, there was no significant difference between a linear or Michaelis–Menten function for the low-CO_2 data, which suggests that full acclimation to a high-pH environment prior to the ^{14}C incubations lessened the negative effect that high pH had on Ci assimilation.

Based on our simulation, the actual carboxylation rate of *Trichodesmium* should be modelled as a function of HCO_3^- and pH. This is because the CO_2 concentration in a saturated HCO_3^-/high-pH environment (i.e. 3.8 mM HCO_3^-, pH=8.4) could be equivalent to a limited HCO_3^-/present-day pH environment (i.e. 1.9 mM HCO_3^-, pH=8.1); which for the aforementioned reasons will impose different constraints on leakage/uptake rates. That said, our experimental data clearly suggested that high-pH-induced processes operating outside of the CCM were contributing to decrease Ci assimilation. Overall, this may allow the Ci assimilation rates of *Trichodesmium* to be ascribed as a function of CO_2 (Fig. 1, see Supplementary Fig. S4), which would be considerably simpler to implement in biogeochemical models of *Trichodesmium* growth and photosynthesis (Hutchins *et al.*, 2013) than a HCO_3^--response curve in which the kinetic constants (K_m and V_m) are pH-dependent. Further experimental work is needed to assess whether a CO_2 parameterisation is consistent across a more extended range of pH and HCO_3^- conditions than those used in our experiments.

Conclusions

Climate change is driving ocean acidification, which results in higher CO_2 and HCO_3^- concentrations and a decrease in pH. We observed systematic changes in the kinetics of inorganic carbon assimilation of *T. erythraeum* IMS101 in response to acclimation to increasing CO_2 concentrations ranging from low CO_2 (levels at the last glacial maximum) through mid-CO_2 (levels at the end of the 20th century), to high CO_2 (levels predicted for 2050–2100). Extrapolating these responses to future scenarios of the natural environment should take into account the fact that our findings were obtained using acclimation experiments whereas *Trichodesmium* may adapt to future conditions (Hutchins *et al.*, 2015), that variability may exist between strains and clades (Hutchins *et al.*, 2013), and that there will be additional effects of integrated abiotic variables (e.g. light and temperature) and nutrients (e.g. P and Fe) on *Trichodesmium* productivity (Walworth *et al.*, 2016; Boatman *et al.*, 2018*a*, 2018*b*).

In the context of the open oceans, our results indicate that nutrient-replete net photosynthesis and growth rates of *T. erythraeum* IMS101 would have been severely CO_2-limited at the last glacial maximum relative to current conditions. However, future increases in CO_2 (i.e. 720 μmol mol^{-1}) may not significantly increase its growth and productivity, although we note that other studies have reported a stimulation of growth and photosynthesis by increasing CO_2 beyond current ambient concentrations (Hutchins *et al.*, 2007; Levitan *et al.*, 2007, 2010). On the other hand, we did observe that growth under high CO_2 will increase key stoichiometric ratios (N:P and C:P). Increases of N:P and C:P in *Trichodesmium*-dominated oceanic regimes may affect bacterial and zooplankton metabolism, the pool of bioavailable nitrogen, the depth at which sinking organic matter is remineralised, and consequently carbon sequestration via the biological carbon pump (Mulholland *et al.*, 2004; McGillicuddy, 2014). These responses could serve as a negative feedback to climate change by increasing new N and C production and thereby increasing the organic carbon sinking to the deep ocean.

Supplementary data

Supplementary data are available at *JXB* online.

Information SI. Calculation of inorganic carbon speciation.

Information SII. Preparation of medium for CO_2-response curves where TIC was varied at fixed pH.

Information SIII. Preparation of medium for CO_2-response curves where pH was varied at fixed TIC.

Table S1. Recent literature on the C- and N_2-fixation rates and elemental stoichiometry of *T. erythraeum* IMS101 in response to CO_2, temperature, and light.

Table S2. The Chl *a*-specific curve-fitting parameter values of the carbon assimilation–CO_2-response curves when the 'TIC varied/pH fixed' and 'pH varied/TIC fixed' data were modelled separately.

Table S3. The carbon-specific curve-fitting parameter values of the carbon assimilation–CO_2-response curves when the 'TIC varied/pH fixed' and 'pH varied/TIC fixed' data were modelled separately.

Fig. S1. The effect of filtration/re-suspension and incubation on photosynthetic efficiency.

Fig. S2. The inorganic carbon chemistry of the culture vessels over a diurnal period.

Fig. S3. The modelled rates of carboxylation, CO_2 leakage, HCO_3^-, uptake and HCO_3^- leakage for a *Trichodesmium* cell.

Fig. S4. The Chl *a*-specific curve fits of the carbon assimilation–CO_2-response curves when the 'TIC varied/pH fixed' and 'pH varied/TIC fixed' data were modelled together.

Fig. S5. The Chl *a*- and carbon-specific curve fits of the carbon assimilation–CO_2-response curves when the 'TIC varied/pH fixed' and 'pH varied/TIC fixed' data were modelled seperately.

Fig. S6. The Chl *a*- and carbon-specific curve fits of the carbon assimilation–CO_2-response curves of the low-CO_2 treatment for the 'TIC varied/pH fixed' data.

Fig. S7. The Chl *a*- and carbon-specific curve fits of the carbon assimilation–CO_2-response curves of the low-CO_2 treatment for the 'pH varied/TIC fixed' data.

Fig. S8. The Chl *a*- and carbon-specific curve fits of the carbon assimilation–CO_2-response curves of the mid-CO_2 treatment for the 'TIC varied/pH fixed' data.

Fig. S9. The Chl *a*- and carbon-specific curve fits of the carbon assimilation–CO_2-response curves of the mid-CO_2 treatment for the 'pH varied/TIC fixed' data.

Fig. S10. The Chl *a*- and carbon-specific curve fits of the carbon assimilation–CO_2-response curves of the high-CO_2 treatment for the 'TIC varied/pH fixed' data.

Fig. S11. The Chl *a*- and carbon-specific curve fits of the carbon assimilation–CO_2-response curves of the high-CO_2 treatment for the 'pH varied/TIC fixed' data.

Fig. S12. A bioimage of *T. erythraeum* IMS101 filaments cultured at mid-CO_2, saturating light, and optimal temperature.

Acknowledgements

Tobias G. Boatman was supported by a UK Natural Environment Research Council PhD studentship (NE/J500379/1 DTB).

References

Badger MR, Andrews TJ. 1987. Co-evolution of Rubisco and CO_2 concentrating mechanisms. In: Biggins J, ed. Progress in photosynthesis research. Dordrecht: Springer, 601–609.

Badger MR, Andrews TJ, Whitney S, Ludwig M, Yellowlees DC, Leggat W, Price GD. 1998. The diversity and coevolution of Rubisco, plastids, pyrenoids, and chloroplast-based CO_2-concentrating mechanisms in algae. Canadian Journal of Botany **76,** 1052–1071.

Badger MR, Hanson D, Price GD. 2002. Evolution and diversity of CO_2 concentrating mechanisms in cyanobacteria. Functional Plant Biology **29,** 161–173.

Badger MR, Palmqvist K, Yu JW. 1994. Measurement of CO_2 and HCO_3^- fluxes in cyanobacteria and microalgae during steady-state photosynthesis. Physiologia Plantarum **90,** 529–536.

Badger MR, Price GD. 2003. CO_2 concentrating mechanisms in cyanobacteria: molecular components, their diversity and evolution. Journal of Experimental Botany **54,** 609–622.

Badger MR, Price GD, Long BM, Woodger FJ. 2006. The environmental plasticity and ecological genomics of the cyanobacterial CO_2 concentrating mechanism. Journal of Experimental Botany **57,** 249–265.

Barcelos e Ramos J, Biswas H, Schulz KG, LaRoche J, Riebesell U. 2007. Effect of rising atmospheric carbon dioxide on the marine nitrogen fixer *Trichodesmium*. Global Biogeochemical Cycles **21,** GB2028.

Behrenfeld MJ, Halsey KH, Milligan AJ. 2008. Evolved physiological responses of phytoplankton to their integrated growth environment. Philosophical Transactions of the Royal Society of London. Series B, Biological sciences **363,** 2687–2703.

Berman-Frank I, Lundgren P, Chen YB, Küpper H, Kolber Z, Bergman B, Falkowski P. 2001. Segregation of nitrogen fixation and oxygenic photosynthesis in the marine cyanobacterium *Trichodesmium*. Science **294,** 1534–1537.

Boatman TG, Lawson T, Geider RJ. 2017. A key marine diazotroph in a changing ocean: the interacting effects of temperature, CO_2 and light on the growth of *Trichodesmium erythraeum* IMS101. PLoS ONE **12,** e0168796.

Boatman TG, Davey PA,Lawson T, Geider RJ. 2018a. The physiological cost of diazotrophy for *Trichodesmium erythraeum* IMS101. PLoS ONE **13,** e0195638.

Boatman TG, Oxborough K,Gledhill M,Lawson T, Geider RJ. 2018b. An integrated response of *Trichodesmium erythraeum* IMS101 growth and photo-physiology to iron, CO_2, and light intensity. Frontiers in Microbiology **9,** 624.

Bronk DA, Ward BB. 2000. Magnitude of dissolved organic nitrogen release relative to gross nitrogen uptake in marine systems. Limnology and Oceanography **45,** 1879–1883.

Capone DG, Burns JA, Montoya JP, Subramaniam A, Mahaffey C, Gunderson T, Michaels AF, Carpenter EJ. 2005. Nitrogen fixation by *Trichodesmium* spp.: an important source of new nitrogen to the tropical and subtropical North Atlantic Ocean. Global Biogeochemical Cycles **19,** GB2024.

Chen YB, Zehr JP, Mellon M. 1996. Growth and nitrogen fixation of the diazotrophic filamentous nonheterocystous cyanobacterium *Trichodesmium* sp. IMS 101 in defined media: evidence for a circadian rhythm. Journal of Phycology **32,** 916–923.

Collos Y, Mornet F, Sciandra A, Waser N, Larson A, Harrison P. 1999. An optical method for the rapid measurement of micromolar concentrations of nitrate in marine phytoplankton cultures. Journal of Applied Phycology **11,** 179–184.

Davis CS, McGillicuddy DJ Jr. 2006. Transatlantic abundance of the N_2-fixing colonial cyanobacterium *Trichodesmium*. Science **312,** 1517–1520.

Eichner M, Thoms S, Kranz SA, Rost B. 2015. Cellular inorganic carbon fluxes in *Trichodesmium*: a combined approach using measurements and modelling. Journal of Experimental Botany **66,** 749–759.

Garcia NS, Fu FX, Breene CL, Bernhardt PW, Mulholland MR, Sohm JA, Hutchins DA. 2011. Interactive effects of irradiance and CO_2 on CO_2 fixation and N_2 fixation in the diazotroph *Trichodesmium erythraeum* (Cyanobacteria). Journal of Phycology **47,** 1292–1303.

Geider RJ, Moore CM, Ross ON. 2009. The role of cost–benefit analysis in models of phytoplankton growth and acclimation. Plant Ecology and Diversity **2,** 165–178.

Hong H, Shen R, Zhang F, *et al*. 2017. The complex effects of ocean acidification on the prominent N_2-fixing cyanobacterium *Trichodesmium*. Science **356,** 527–531.

Hutchins DA, Fu F-X, Webb EA, Walworth N, Tagliabue A. 2013. Taxon-specific response of marine nitrogen fixers to elevated carbon dioxide concentrations. Nature Geoscience **6,** 790–795.

Hutchins DA, Fu F-X, Zhang Y, Warner M, Feng Y, Portune K, Bernhardt P, Mulholland M. 2007. CO_2 control of *Trichodesmium* N_2 fixation, photosynthesis, growth rates, and elemental ratios: implications for past, present, and future ocean biogeochemistry. Limnology and Oceanography **52,** 1293–1304.

Hutchins DA, Walworth NG, Webb EA, Saito MA, Moran D, McIlvin MR, Gale J, Fu F-X. 2015. Irreversibly increased nitrogen fixation in *Trichodesmium* experimentally adapted to elevated carbon dioxide. Nature Communications **6,** 8155.

Kaplan A, Reinhold L. 1999. CO_2 concentrating mechanisms in photosynthetic microorganisms. Annual Review of Plant Physiology and Plant Molecular Biology **50,** 539–570.

Kranz SA, Eichner M, Rost B. 2011. Interactions between CCM and N_2 fixation in *Trichodesmium*. Photosynthesis Research **109,** 73–84.

Kranz SA, Levitan O, Richter KU, Prásil O, Berman-Frank I, Rost B. 2010. Combined effects of CO_2 and light on the N_2-fixing cyanobacterium *Trichodesmium* IMS101: physiological responses. Plant Physiology **154,** 334–345.

Kranz SA, Sültemeyer D, Richter KU, Rost B. 2009. Carbon acquisition in *Trichodesmium*: the effect of pCO_2 and diurnal changes. Limnology and Oceanography **54,** 548–559.

Levitan O, Brown CM, Sudhaus S, Campbell D, LaRoche J, Berman-Frank I. 2010. Regulation of nitrogen metabolism in the marine diazotroph *Trichodesmium* IMS101 under varying temperatures and atmospheric CO_2 concentrations. Environmental Microbiology **12,** 1899–1912.

Levitan O, Rosenberg G, Setlik I, Setlikova E, Grigel J, Klepetar J, Prasil O, Berman-Frank I. 2007. Elevated CO_2 enhances nitrogen fixation and growth in the marine cyanobacterium *Trichodesmium*. Global Change Biology **13,** 531–538.

Li W, Dickie P. 1991. Light and dark ^{14}C uptake in dimly-lit oligotrophic waters: relation to bacterial activity. Journal of Plankton Research **13,** 29–44.

Mangan NM, Brenner MP. 2014. Systems analysis of the CO_2 concentrating mechanism in cyanobacteria. eLIFE **3,** e02043.

Mangan NM, Flamholz A, Hood RD, Milo R, Savage DF. 2016. pH determines the energetic efficiency of the cyanobacterial CO_2 concentrating mechanism. Proceedings of the National Academy of Sciences, USA **113,** E5354–E5362.

McGillicuddy DJ. 2014. Do *Trichodesmium* spp. populations in the North Atlantic export most of the nitrogen they fix? Global Biogeochemical Cycles **28,** 103–114.

Mulholland MR, Bronk DA, Capone DG. 2004. Dinitrogen fixation and release of ammonium and dissolved organic nitrogen by *Trichodesmium* IMS101. Aquatic Microbial Ecology **37,** 85–94.

Myklestad S, Swift E. 1998. A new method for measuring soluble cellular organic content and a membrane property, T_m, of planktonic algae. European Journal of Phycology **33,** 333–336.

Price GD, Badger MR, Woodger FJ, Long BM. 2008. Advances in understanding the cyanobacterial CO_2-concentrating-mechanism (CCM): functional components, Ci transporters, diversity, genetic regulation and prospects for engineering into plants. Journal of Experimental Botany **59,** 1441–1461.

Raven JA. 1981. Nutrient transport in microalgae. Advances in Microbial Physiology **21,** 47–226.

Raven J, Caldeira K, Elderfield H, Hoegh-Guldberg O, Liss P, Riebesell U, Shepherd J, Turley C, Watson A. 2005. Ocean acidification due to increasing atmospheric carbon dioxide. Policy Document 12/05. London: The Royal Society.

Ritchie R. 2008. Universal chlorophyll equations for estimating chlorophylls *a*, *b*, *c*, and *d* and total chlorophylls in natural assemblages of photosynthetic organisms using acetone, methanol, or ethanol solvents. Photosynthetica **46,** 115–126.

Schwarz R, Reinhold L, Kaplan A. 1995. Low activation state of ribulose-1,5-bisphosphate carboxylase/oxygenase in carboxysome-defective *Synechococcus* mutants. Plant Physiology **108,** 183–190.

Solorzano L. 1969. Determination of ammonia in natural waters by the phenol hypochlorite method. Limnology and Oceanography **14,** 799–801.

Solorzano L, Sharp JH. 1980. Determination of total dissolved phosphorus and particulate phosphorus in natural waters. Limnology and Oceanography **25,** 754–758.

Steemann Nielsen E, Jensen EA. 1957. Primary oceanic production. The autotrophic production of organic matter in the oceans. In: Bruun AF, Greve SV, Spärck R, eds. Galathea Report, vol. 1. Copenhagen: The Galathea Committee, 49–135.

Walworth NG, Fu FX, Webb EA, Saito MA, Moran D, McIlvin MR, Lee MD, Hutchins DA. 2016. Mechanisms of increased *Trichodesmium* fitness under iron and phosphorus co-limitation in the present and future ocean. Nature Communications **7,** 12081.

Welschmeyer NA. 1994. Fluorometric analysis of chlorophyll *a* in the presence of chlorophyll *b* and pheopigments. Limnology and Oceanography **39,** 1985–1992.

Zeebe RE, Wolf-Gladrow D, Jansen H. 1999. On the time required to establish chemical and isotopic equilibrium in the carbon dioxide system in seawater. Marine Chemistry **65,** 135–153.

Zeebe RE, Wolf-Gladrow DA. 2001. CO_2 in seawater: equilibrium, kinetics, isotopes. Elsevier Oceanography Series 65. Elsevier.